Dyes and Pigments 126 (2016) 76–85

Contents lists available at ScienceDirect

Dyes and Pigments

journal homepage: www.elsevier.com/locate/dyepig

A simple structural modification to thiazole orange to improve the selective detection of G-quadruplexes

Rui-Jun Guo [a], Jin-Wu Yan [b], Shuo-Bin Chen [a], Lian-Quan Gu [a], Zhi-Shu Huang [a], Jia-Heng Tan [a, *]

[a] School of Pharmaceutical Sciences, Sun Yat-sen University, Guangzhou 510006, China
[b] School of Bioscience and Bioengineering, South China University of Technology, Guangzhou 510006, China

ARTICLE INFO

Article history:
Received 23 July 2015
Received in revised form
12 November 2015
Accepted 14 November 2015
Available online 26 November 2015

Keywords:
G-quadruplex
Thiazole orange
Structural modification
Fluorescence probe
Selectivity
Binding mode

ABSTRACT

Thiazole orange is a commonly used cyanine dye for binding to nucleic acids. Recently, it has been used for the detection of G-quadruplexes. However, thiazole orange is non-selective for G-quadruplex and other nucleic acids, thus hampering its further application. Herein, we designed and synthesized new fluorescent probes by incorporating hydrocarbon rings into the chromophore of thiazole orange. This simple modification dramatically improved selective binding to certain G-quadruplexes. The most promising probe, the cyclopentane fused analogue, exhibited significant fluorescence enhancement when treated with G-quadruplexes but retained weak fluorescence in the presence of double-stranded and single-stranded DNA. The cyclopentane fused probe also displayed considerable selectivity for parallel G-quadruplexes. These modifications reduced the quantum yield of thiazole orange. Further study of the mechanism revealed that the introduction of a hydrocarbon ring altered the planarity of the chromophore as well as the binding affinities for G-quadruplexes, and therefore, influenced the ability to detect G-quadruplexes.

1. Introduction

Thiazole orange (**TO**, Fig. 1) is an exceptional asymmetric cyanine dye. It is essentially non-fluorescent in aqueous solution and obtains intense fluorescence when bonded to double-stranded nucleic acids [1,2]. These unique properties make **TO** particularly useful for the detection of double-stranded nucleic acids in a variety of techniques. Examples include the detection of PCR products in real time, staining double-stranded DNA in agarose gels and capillary electrophoresis, and applications in fluorescent in situ hybridization [3–6].

In addition to double-stranded nucleic acids, **TO** is used for the detection of G-quadruplexes (G4s) [7,8]. G-quadruplexes are unique four-stranded structures that are formed by guanine-rich nucleic acid sequences. The building blocks of G-quadruplexes are G-quartets, which stack up on top of each other to form secondary DNA structures. G-quadruplexes are widely dispersed in eukaryotic genomes and can be divided into two main topologies: parallel and antiparallel structures [9–11]. During the past two decades, G-quadruplex structures have attracted considerable attention because of their biological significance and potential applications in supramolecular chemistry [12–14]. The ever-increasing interest in G-quadruplexes has promoted the development of rapid and simple approaches for the selective detection of these structures. Thus, the discovery of selective fluorescent probes for G-quadruplexes has become an extremely active area of research [15–25]. Notably, unlike the commercially available dye thioflavin T (ThT) which is a selective G-quadruplex probe [26–28], **TO** is non-selective for double-stranded and G-quadruplex nucleic acids. However, it may offer an attractive template for the design of selective fluorescent probes for G-quadruplexes. Successful examples include the bisquinolinium/**TO** conjugate and the benzofuroquinolinium/**TO** conjugate [29,30].

As shown in Fig. 1, the conjugates includes the assembly of the **TO** and the G-quadruplex binding small molecule all in a fusion scaffold with the aim of combining their advantages. These fluorescent probes exhibit distinct selectivity for G-quadruplexes over double-stranded nucleic acids. However, the conjugation strategy requires a suitable molecular framework to accommodate the **TO** chromophore. One relevant example is our previous work on the

* Corresponding author.
E-mail address: tanjiah@mail.sysu.edu.cn (J.-H. Tan).

http://dx.doi.org/10.1016/j.dyepig.2015.11.010
0143-7208/

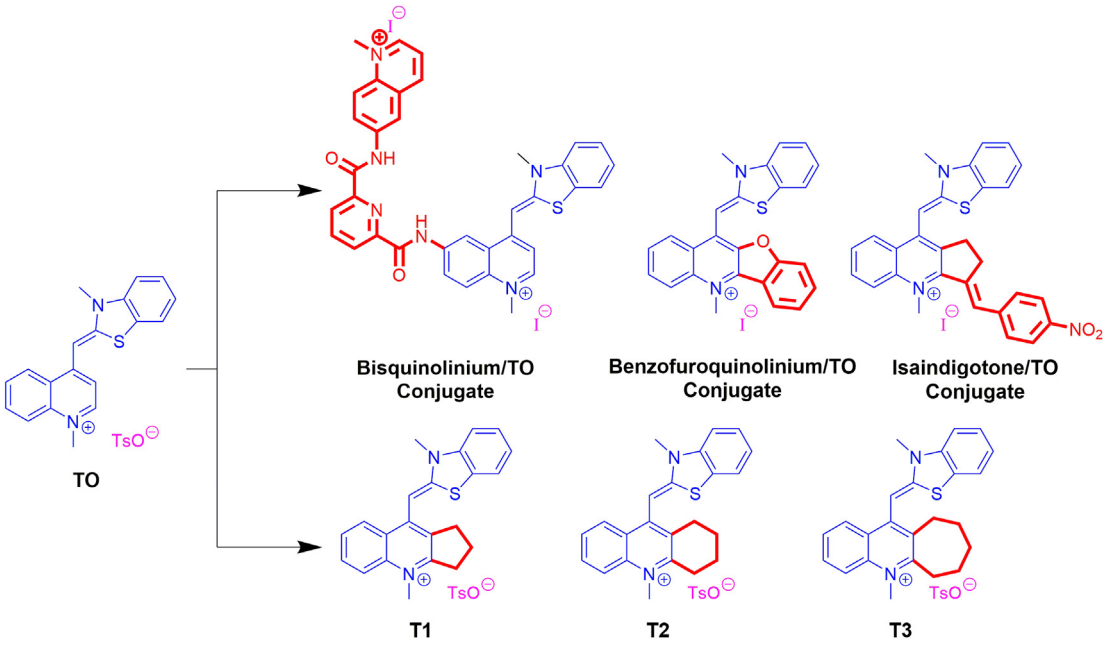

Fig. 1. Structures of **TO**, the bisquinolinium/**TO** conjugate, the benzofuroquinolinium/**TO** conjugate, the isaindigotone/**TO** conjugate and the **TO**-derived compounds: **T1**, **T2** and **T3**.

isaindigotone/**TO** conjugate [31]. This compound exhibits a high selectivity for the G-quadruplex, but it is non-fluorescent upon combination with the G-quadruplex. Incorporation of **TO** into the isaindigotone framework surprisingly eliminates the fluorescent properties of **TO**. Accordingly, it led us to reconsider the modification strategy, and we developed a G-quadruplex-specific fluorescent probe using a more simple structural modification to the **TO** scaffold.

Based on our experience in developing selective G-quadruplex binding ligands, we introduced some simple moieties to the **TO** scaffold [32–34]. Herein, we present a new series of **TO**-derived compounds: **T1**, **T2** and **T3**. Compared with **TO**, these compounds bear a hydrocarbon ring that has been suggested to be an important factor in the binding of small molecules to a G-quadruplex. Their photophysical properties were examined alone and in the presence of different nucleic acids. In addition, molecular modeling approaches were employed to assist in understanding the differences and the relevant mechanism.

2. Experimental methods

2.1. Synthesis and characterization

^{1}H and ^{13}C NMR spectra were recorded using TMS as the internal standard in $CDCl_3$ or DMSO-d_6 using a Bruker BioSpin GmbH spectrometer at 400 MHz and 101 MHz, respectively. IR spectra were determined on a Bruker Tensor 37 infrared spectrophotometer. Mass spectra (MS) were recorded on a Shimadzu LCMS-2010A instrument with an ESI or ACPI mass selective detector, and high resolution mass spectra (HRMS) were obtained on a Shimadzu LCMS-IT-TOF. Melting points (Mp) were determined using a SRS OptiMelt automated melting point instrument without correction. Flash column chromatography was performed with silica gel (200–300 mesh) purchased from Qingdao Haiyang Chemical Co. Ltd. The purity of the synthesized compound was confirmed to be higher than 95% via analytical HPLC that was performed with a dual pump Shimadzu LC-20 AB system equipped with a Ultimate XB-C18 column (4.6 × 250 mm, 5 μm). All chemicals were purchased from commercial sources unless otherwise specified. All of the solvents were of analytical reagent grade and were used without further purification. The 2,3-dimethylbenzothiazolium tosylate was synthesized according to a previous report [35].

2.1.1. 9-Chloro-2,3-dihydro-1H-cyclopenta[b]quinolone (1)

To a stirred solution of 2-aminobenzoic acid (1.37 g, 10 mmol) and cyclopentanone (1.5 mL, 16.9 mmol) cooled in an ice bath, $POCl_3$ (11 mL) was carefully added and the mixture was refluxed for 5 h. After cooling to room temperature, the mixture was concentrated to give a slurry. The residue was then diluted with EtOAc, and neutralized with NaOH solution. The organic layer was dried over anhydrous $MgSO_4$. After concentration, the resulting residue was purified by flash chromatography with EtOAc: petroleum ether (1:3–1:5) to afford a white solid **1** (1.05 g, 52%). ^{1}H NMR (400 MHz, $CDCl_3$) δ 8.17 (dd, J = 8.3, 1.0 Hz, 1H), 8.06 (d, J = 8.4 Hz, 1H), 7.72–7.66 (m, 1H), 7.61–7.55 (m, 1H), 3.26 (t, J = 7.7 Hz, 2H), 3.18 (t, J = 7.5 Hz, 2H), 2.31–2.22 (m, 2H). ESI-MS m/z: 204.0 $[M+H]^+$.

2.1.2. 9-Chloro-1,2,3,4-tetrahydroacridine (2)

The method for the preparation of compound **1** was used by replacing cyclopentanone with cyclohexanone. Compound **2** was synthesized as a white solid (1.07 g, 49%). ^{1}H NMR (400 MHz, $CDCl_3$) δ 8.16 (d, J = 8.3 Hz, 1H), 7.98 (d, J = 8.4 Hz, 1H), 7.66 (t, J = 7.6 Hz, 1H), 7.53 (t, J = 7.3 Hz, 1H), 3.13 (t, J = 5.7 Hz, 2H), 3.02 (t, J = 5.8 Hz, 2H), 2.05–1.91 (m, 4H). ESI-MS m/z: 218.1 $[M+H]^+$.

2.1.3. 11-Chloro-7,8,9,10-tetrahydro-6H-cyclohepta[b]quinoline (3)

The method for the preparation of compound **1** was used by replacing cyclopentanone with cycloheptanone. Compound **3** was synthesized as a white solid (1.12 g, 48%). ^{1}H NMR (400 MHz, $CDCl_3$) δ 8.17 (d, J = 8.2 Hz, 1H), 7.99 (d, J = 8.3 Hz, 1H), 7.67 (t, J = 7.1 Hz, 1H), 7.56 (t, J = 7.6 Hz, 1H), 3.31–3.18 (m, 4H), 1.95–1.87 (m, 2H), 1.86–1.71 (m, 4H). ESI-MS m/z: 232.1 $[M+H]^+$.

2.1.4. (Z)-4-methyl-9-((3-methylbenzo[d]thiazol-2(3H)-ylidene) methyl)-2,3-dihydro-1H-cyclopenta[b]quinolin-4-ium tosylate (*T1*)

A mixture of **1** (0.41 g, 2.0 mmol), methyl tosylate (0.9 mL, 6.0 mmol), and toluene (1 mL) was heated at 110 °C for 6 h. After cooling to room temperature, a solution containing 2,3-

dimethylbenzothiazolium tosylate (0.5 g, 1.5 mmol) in 1 mL ethanol and $KHCO_3$ (0.20 g, 2 mmol) in 1 mL water was added. Then, the solution was stirred at reflux for another 1 h. After concentration, the residue was diluted with CH_2Cl_2. The organic layer was dried over anhydrous $MgSO_4$. The CH_2Cl_2 was removed and the residue was purified by flash chromatography with methanol: CH_2Cl_2 (1:20) to afford brownish black solid **T1** (0.11 g, 11%). Mp: 102–105 °C; ^{1}H NMR (400 MHz, DMSO-d_6) δ 8.47 (d, J = 8.1 Hz, 1H), 8.28 (d, J = 8.6 Hz, 1H), 8.02 (t, J = 7.6 Hz, 1H), 7.77 (t, J = 7.3 Hz, 1H), 7.67 (d, J = 7.4 Hz, 1H), 7.51–7.39 (m, 4H), 7.18 (t, J = 7.1 Hz, 1H), 7.09 (d, J = 7.4 Hz, 2H), 6.29 (s, 1H), 4.23 (s, 3H), 3.75 (s, 3H), 3.50 (t, J = 7.2 Hz, 2H), 3.06 (t, J = 7.0 Hz, 2H), 2.33–2.20 (m, 5H). ^{13}C NMR (101 MHz, DMSO-d_6) δ 162.50, 156.66, 147.73, 145.95, 141.31, 137.95, 137.37, 132.82, 130.09, 128.01, 127.91, 127.18, 126.69, 125.44, 123.59, 122.95, 122.85, 122.07, 118.36, 111.10, 86.32, 33.87, 32.87, 31.93, 21.92, 20.70. NOESY experiment showed the correlation between the alkene proton at 6.29 ppm and the N-methyl proton at 3.75 ppm of thiazole, thus the double bond was assigned as the *Z* configuration. IR (cm^{-1}, KBr): 3060, 3019, 2923, 2853, 1648, 1587, 1504, 1372, 1120, 1061, 1033, 1010. Purity: 99.7% by HPLC. HRMS (ESI): calcd for (M-TsO)$^+$ ($C_{31}H_{30}N_3S^+$) 345.1420, found 345.1407.

2.1.5. (Z)-10-methyl-9-((3-methylbenzo[d]thiazol-2(3H)-ylidene) methyl)-1,2,3,4-tetrahydroacridin-10-ium tosylate (*T2*)

The method for the preparation of compound **T1** was used by replacing compound **1** with compound **2**. Compound **T2** was synthesized as a brownish black solid (0.18 g, 17%). Mp: 96–98 °C; ^{1}H NMR (400 MHz, DMSO-d_6) δ 8.39 (dd, J = 8.4, 1.1 Hz, 1H), 8.36 (d, J = 8.9 Hz, 1H), 8.06–8.00 (m, 1H), 7.72 (t, J = 6.3 Hz, 1H), 7.57 (d, J = 7.7 Hz, 1H), 7.46 (d, J = 8.0 Hz, 2H), 7.45–7.37 (m, 2H), 7.16–7.07 (m, 3H), 6.11 (s, 1H), 4.23 (s, 3H), 3.74 (s, 3H), 3.25 (t, J = 6.3 Hz, 2H), 2.93 (t, J = 6.2 Hz, 2H), 2.28 (s, 3H), 1.95–1.80 (m, 4H). ^{13}C NMR (101 MHz, DMSO-d_6) δ 157.59, 154.20, 151.64, 145.80, 141.32, 138.27, 137.46, 133.61, 129.28, 127.95, 127.05, 126.56, 126.27, 125.42, 122.92, 122.27, 121.96, 121.57, 118.74, 110.81, 86.77, 37.25, 32.76, 29.39, 26.60, 21.35, 20.71, 20.54. NOESY experiment showed the correlation between the alkene proton at 6.11 ppm and the N-methyl proton at 3.74 ppm of thiazole, thus the double bond was assigned as the *Z* configuration. IR (cm^{-1}, KBr): 3060, 3015, 2923, 2853, 1646, 1583, 1494, 1353, 1120, 1062, 1033, 1010. Purity: 97.3% by HPLC. HRMS (ESI): calcd for (M-TsO)$^+$ ($C_{31}H_{30}N_3S^+$) 359.1576, found 359.1567.

2.1.6. (Z)-5-methyl-11-((3-methylbenzo[d]thiazol-2(3H)-ylidene) methyl)-7,8,9,10-tetrahydro-6H-cyclohepta[b]quinolin-5-ium tosylate (*T3*)

The method for the preparation of compound **T1** was used by replacing compound **1** with compound **3**. Compound **T3** was synthesized as a brownish black solid (0.15 g, 14%). Mp: 92–94 °C; ^{1}H NMR (400 MHz, DMSO-d_6) δ 8.46 (dd, J = 8.3, 0.9 Hz, 1H), 8.41 (d, J = 8.8 Hz, 1H), 8.09–8.01 (m, 1H), 7.80 (t, J = 6.0 Hz, 1H), 7.51 (d, J = 7.6 Hz, 1H), 7.47 (d, J = 8.0 Hz, 2H), 7.36–7.29 (m, 2H), 7.10 (d, J = 7.9 Hz, 2H), 7.08–7.05 (m, 1H), 6.31 (s, 1H), 4.37 (s, 3H), 3.69 (s, 3H), 3.51–3.47 (m, 2H), 3.24–3.18 (m, 2H), 2.28 (s, 3H), 1.90–1.80 (m, 4H), 1.68–1.60 (m, 2H). ^{13}C NMR (101 MHz, DMSO) δ 162.02, 154.87, 150.25, 145.90, 141.78, 137.86, 137.41, 133.21, 133.13, 128.52, 127.94, 127.61, 126.87, 125.45, 124.35, 122.20, 122.13, 121.75, 119.44, 110.13, 85.15, 32.33, 31.86, 29.58, 29.51, 26.63, 23.63, 20.71. NOESY experiments showed the correlation between the alkene proton at 6.31 ppm and the N-methyl proton at 3.69 ppm of thiazole, thus the double bond was assigned as the *Z* configuration. IR (cm^{-1}, KBr): 3057, 3022, 2922, 2853, 1636, 1584, 1503, 1352, 1119, 1061, 1032, 1010. Purity: 99.6% by HPLC. HRMS (ESI): calcd for (M-TsO)$^+$ ($C_{31}H_{30}N_3S^+$) 373.1733, found 373.1721.

2.2. Materials

All oligonucleotides (Table 1) used in this study were purchased from Invitrogen (China), and their concentrations were determined using the absorbance at 260 nm based on their respective molar extinction coefficients using a NanoDrop 1000 Spectrophotometer (Thermo Scientific, USA). To form the G-quadruplexes, oligonucleotides were annealed in a relevant buffer containing KCl by heating to 95 °C for 5 min, followed by gradual cooling to room temperature. The oligonucleotides were engaged in G-quadruplex formation, and their conformations were determined by circular dichroism (CD) measurements (Fig. S1, Supplementary Data) [11]. Stock solutions of the compounds, **TO**, **T1**, **T2** and **T3** (10 mM), were dissolved in DMSO and stored at −80 °C. Further dilutions of the compounds to working concentrations were prepared in a relevant buffer immediately prior to use.

2.3. UV–Vis and fluorescence spectroscopic studies

The UV–Vis spectra were obtained using a UV-2450 spectrophotometer (Shimadzu, Japan) using a 1 cm path length quartz cuvette. The fluorescence spectra were obtained using a LS-55 luminescence spectrophotometer (Perkin–Elmer, USA). A quartz cuvette with a 2 mm × 10 mm path length was used for the spectra recorded at 10 nm excitation and emission slit widths unless otherwise specified.

For the titration experiment, small aliquots of a stock solution of the samples (oligonucleotides) were added to the solution containing **T1** at a fixed concentration (5 μM) in Tris–HCl buffer (10 mM, pH 7.2) with 100 mM KCl. The final concentration of the sample was varied from 0 to 30 μM. After each sample addition, the reaction was stirred and allowed to equilibrate for at least 1 min, and the fluorescence measurement was obtained at an excitation wavelength of 480 nm. In competition experiments, single-stranded DNA mut-htg21 and double-stranded DNA hairpin were used as the competitors.

The fluorescence quantum yield (Φ_F) of the compound was calculated relative to a standard solution of rhodamine 123 in ethanol (Φ_F = 0.90) and was determined using the following formula: $\Phi_u = \Phi_s (A_s/A_u) \times (I_u/I_s)$, where Φ is the fluorescence quantum yield, I is the measured integrated emission intensity, and A is the optical density (absorbance). The u refers to the compound of an unknown quantum yield, and s refers to the reference compound (Rhodamine 123) of a known quantum yield. The fluorescence spectra were recorded at 10 nm excitation and emission slit widths for the determination of Φ.

The LOD values of **T1** for different nucleic acids in solution were calculated on the basis of the equation LOD = $K \times S_b/m$. The K value is generally taken to be 3 according to the IUPAC recommendation. The S_b value represents the standard deviation for multiple measurements (n = 20) of blank solution. The m value is the slope of the calibration curve, which was derived from the linear range of a **T1** fluorescence titration curve with different nucleic acids and standards for the sensitivity of this method.

2.4. Polyacrylamide gel electrophoresis (PAGE) studies

Different oligonucleotides were loaded onto a 20% bisacrylamide gel in 0.5 × TBE buffer containing 12.5 mM KCl and 12.5 mM NaCl, and electrophoresed at 4 °C. The oligonucleotides were stained with **T1** (30 μmol/L, 20 min), or by the commercial staining agent GelRed (1×, 20 min). DNA fragments were visualized under UV light and photographed by using AlphaImager EC (ProteinSimple).

Table 1
The DNA samples used in this study.

Name	Sequence	Structure in K^+ solution
Pu27	5′-d(TGGGGAGGGTGGGGAGGGTGGGGAAGG)-3′	Parallel G4 DNA
RET	5′-d(GGGGCGGGGCGGGGCGGGGG)-3′	Parallel G4 DNA
Bcl-2	5′-d(GGGCGGGCGCGGGAGGAAGGGGGCGGG)-3′	Parallel G4 DNA
c-kit2	5′-d(CGGGCGGGCGCGAGGGAGGGT)-3′	Parallel G4 DNA
c-kit1	5′-d(AGGGAGGGCGCTGGGAGGAGGG)-3′	Parallel G4 DNA
Htg21	5′-d(GGGTTAGGGTTAGGGTTAGGG)-3′	Antiparallel G4 DNA
TBA	5′-d(GGTTGGTGTGGTTGG)-3′	Antiparallel G4 DNA
ds26	5′-d(CAATCGGATCGAATTCGATCCGATTG)-3′	Double-Stranded DNA
Hairpin	5′-d(CGCGCGCGTTTTCGCGCGCG)-3′	Double-Stranded DNA
mut-Pu27	5′-d(TGAAGAAGGTGAGGAAGATAGAGAAGG)-3′	Single-Stranded DNA
mut-htg21	5′-d(GAGTTAGAGTTAGAGTTAGAG)-3′	Single-Stranded DNA
SPR-Pu27	5′-biotin-d(ACGTACGTGGGGAGGGTGGGGAGGGTGGGGAAGGTGGGG)-3′	Parallel G4 DNA
SPR-htg21	5′-biotin-d(GTTAGGGTTAGGGTTAGGGTTAGGGTTAGG)-3′	Antiparallel G4 DNA
SPR-dsDNA	5′-biotin-d(TTCGCGCGCGTTTTCGCGCGCG)-3′	Double-Stranded DNA
SPR-ssDNA	5′-biotin-d(AGTTAGAGTTAGAGTTAGAGTTAGAGTTAG)-3′	Single-Stranded DNA

2.5. Surface plasmon resonance (SPR) studies

The SPR measurements were performed on a ProteOn XPR36 Protein Interaction Array system (Bio-Rad Laboratories, Hercules, CA) using a Neutravidin-coated GLH sensor chip. The biotinylated oligonucleotides (SPR-Pu27, SPR-htg21, SPR-dsDNA, SPR-ssDNA) were attached to the chip. In a typical experiment, biotinylated DNA was folded in filtered and degassed running buffer (50 mM Tris–HCl, 100 mM KCl, pH 7.2). The DNA samples were then captured (~1000 RU) in four flow cells, and one flow cell was used as the blank. Solutions of the compounds, **TO**, **T1**, **T2** and **T3**, were prepared with running buffer through serial dilutions of the stock solution. Five concentrations were injected simultaneously at a flow rate of 50 μL/min for 400 s during the association phase, followed with 400 s during the dissociation phase at 25 °C. The GLH sensor chip was regenerated with a short injection of 50 mM NaOH between consecutive measurements. The final graphs were obtained by subtracting blank sensorgrams from the different DNA sensorgrams. The data were analyzed with ProteOn manager software using the Langmuir model to fit the kinetic data.

2.6. Molecular modeling studies

The structures of compounds **TO**, **T1**, **T2** and **T3** were constructed and optimized with Gaussian 03 using the HF/6–31G* basis set. The parallel Pu27-derived NMR G-quadruplex structure, Pu24I, with TMPyP4 and a antiparallel NMR G-quadruplex structure for the human telomeric with telomestatin were used as the templates (PDB ID: 2A5R and 2MB3) for the docking studies [36,37]. The docking simulations were performed using Schrodinger software for the binding site based on the reference ligands.

3. Results and discussion

3.1. Synthesis of the *TO*-derived compounds: *T1*, *T2* and *T3*

The **TO**-derived compounds, **T1**, **T2** and **T3**, were synthesized following the procedure reported previously by our group [31]. As shown in Scheme 1, compound **1** was prepared via the condensation of 2-aminobenzoic acid and cyclopentanone in the presence of $POCl_3$. The treatment of **1** with methyl 4-methylbenzenesulfonate yielded the *N*-methylquinolinium intermediate product. Without further purification, the crude product was treated with 2,3-dimethylbenzothiazolium tosylate to produce the final compound, **T1**. The synthesis of **T2** and **T3** was accomplished following the same procedures but from cyclohexanone and cycloheptanone, respectively. Compounds **T1**, **T2** and **T3** were assigned as the *Z* configuration on the basis of NOESY experiments.

3.2. Optical properties of the *TO*-derived compounds: *T1*, *T2*, and *T3*

The optical properties of newly synthesized compounds, **T1**, **T2**, and **T3**, were first investigated in different solvents. Compound **TO** was used as the reference. As shown in Fig. 2, the absorbance of these compounds was weak in aqueous solution but stronger in organic solutions. Notably, the absorption spectrum of **TO** in water exhibited a strong positive band at approximately 505 nm, a shoulder peak at 480 nm, and a minor positive band at approximately 425 nm. This absorbance pattern was quite different from those of compounds **T1**, **T2**, and **T3**, which exhibited only a major positive band at approximately 515 nm. Similar results could be found in other solvents. From the literature, the absorption bands at approximately 480 and 425 nm can be assigned to the H-dimer and higher H-aggregates of **TO**, respectively, in comparison with the monomer band at approximately 505 nm [38,39]. The different absorbance patterns indicated that **T1**, **T2**, and **T3** exhibited weaker propensity to aggregate in aqueous solution than **TO**.

With an increase in concentration, both **TO** and **T1** showed increased absorption intensity, whereas their band profiles were quite different in the normalized absorption spectra at different concentrations. As shown in Fig. 3A and B, absorption banks of **TO** at approximately 480 and 425 nm gradually increased. However, shape and position of absorption banks of **T1** changed little. Besides, variations of absorption intensity of **T1** (0–100 μM) strictly followed the Beer–Lambert law as compared to those of **TO** (Fig. 3C and D). All of these results reinforce the conclusion that **T1** exhibited weaker propensity to aggregate in buffer solution than **TO**. Then, the fluorescence properties of compounds **T1**, **T2**, and **T3** in different solvents were studied. Interestingly, their fluorescence emissions were extremely week in both aqueous and organic solutions. Thus, the maximum in the fluorescence emission spectrum could not be determined.

3.3. Screening of the *TO*-derived compounds: *T1*, *T2*, and *T3*

To identify the most promising **TO**-derived fluorescent probe, compounds **T1**, **T2**, and **T3** were screened for their fluorescence enhancement and selectivity for G-quadruplexes. Compound **TO** was used as the reference. Three representative oligonucleotides, including the single-stranded DNA mut-htg21, the double-stranded DNA hairpin and the G-quadruplex DNA formed by the oligonucleotide Pu27, were employed in the assays. UV–Vis

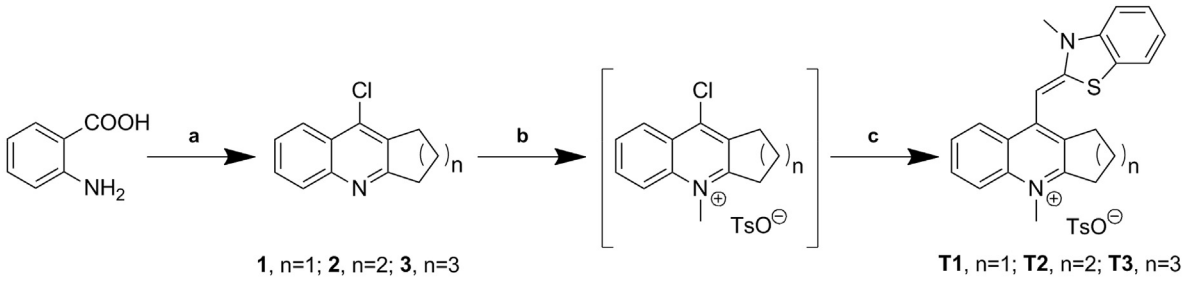

[a] Reagents and conditions: (a) cyclopentanone or cyclohexanone or cycloheptanone, $POCl_3$, reflux; (b) methyl tosylate, toluene, 110 °C; (c) 2,3-dimethylbenzothiazolium tosylate, toluene/ethanol/H_2O, $KHCO_3$, reflux.

Scheme 1. Synthesis of compounds **T1**, **T2** and **T3**.[a]

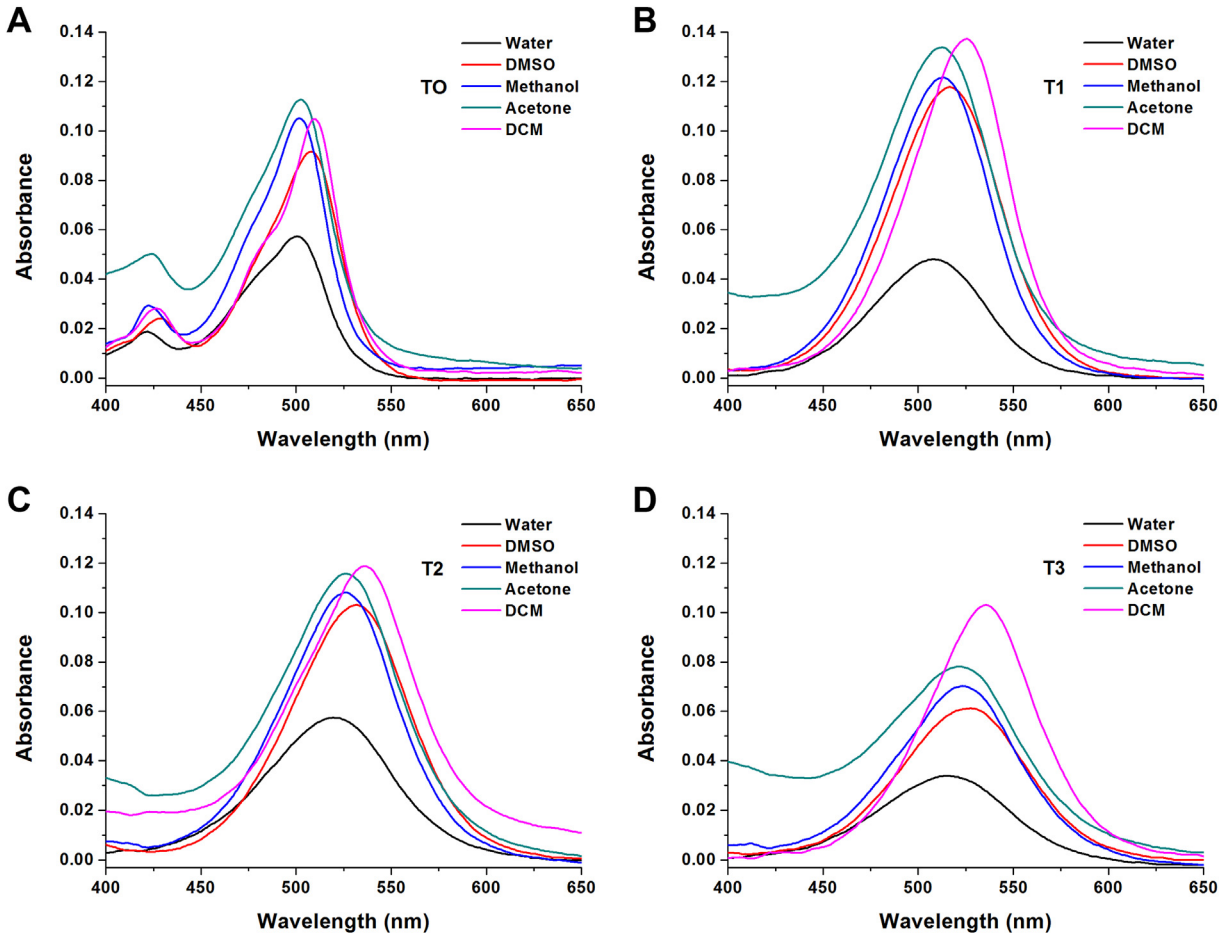

Fig. 2. Absorption spectra of 5 μM of **TO** (A), **T1** (B), **T2** (C) and **T3** (D) in different solvents.

titration experiments were first performed to identify isosbestic point at which fluorescence was generally excited (Fig. S2, Supplementary Data). However, differences in wavelength between position of the isosbestic point and maximum of the emission spectrum were too close. To reduce the interference from excitation and ensure the integrity of fluorescence spectra, fluorescence measurement was obtained at an excitation wavelength of 480 nm. As shown in Fig. 4, the fluorescence emissions of **T1**, **T2**, and **T3** alone in buffer were weak, even in the presence of single-stranded and double-stranded DNA. In contrast, all of the compounds displayed fluorescence enhancement upon addition of G-quadruplex Pu27. **T1** was the most promising compound due to its much stronger fluorescence enhancement than **T2** or **T3** and more selective fluorescence response for the G-quadruplex than **TO**. As a result, **T1** was chosen for further detailed investigation.

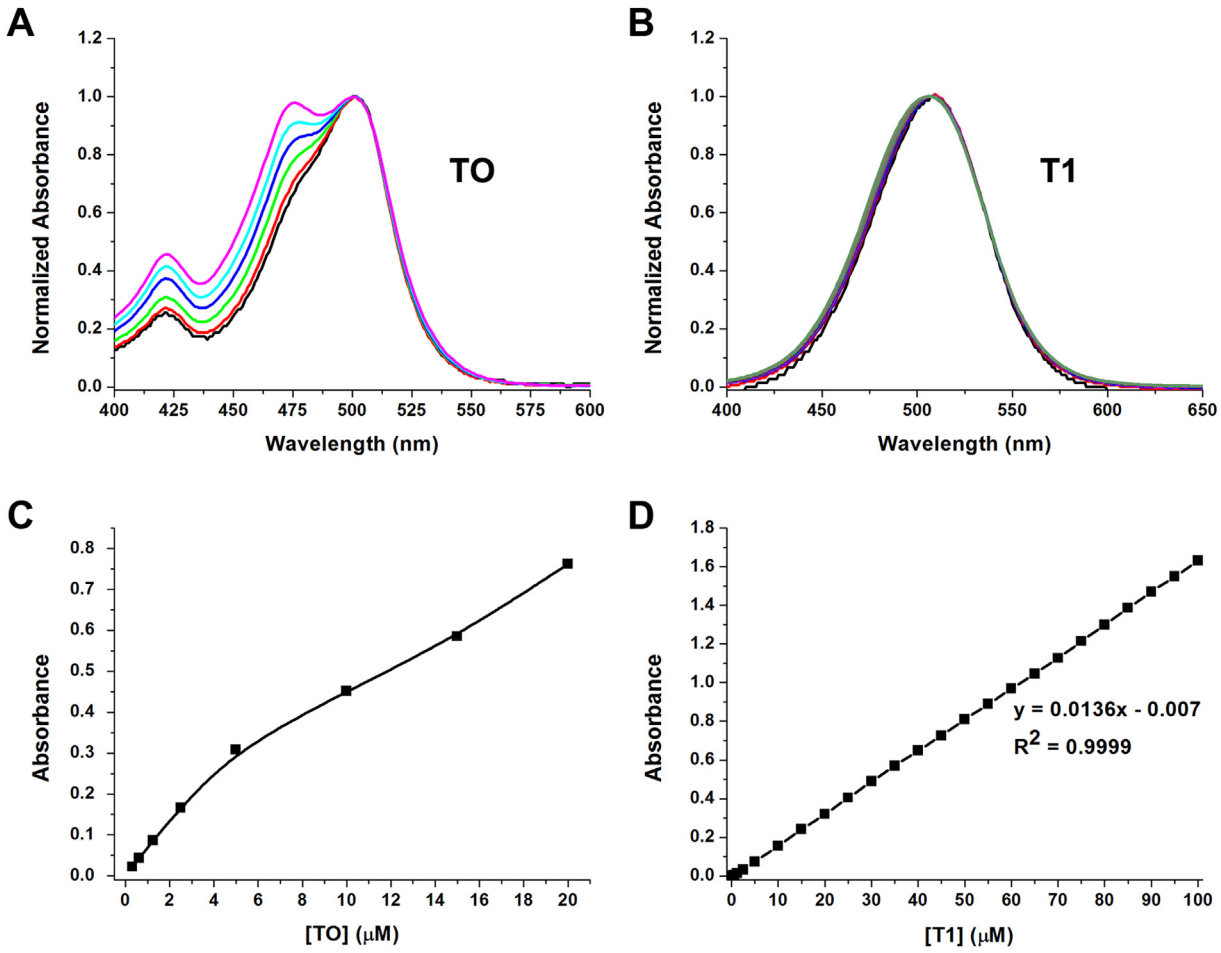

Fig. 3. Normalized absorption spectra of 1.25–20 μM of **TO** (A) and 5–100 μM of **T1** (B), and their corresponding concentration-dependent absorbance at 505 nm for **TO** (C) and **T1** (D) in buffer solution (10 mM Tris–HCl buffer, 100 mM KCl, pH 7.2).

*3.4. Fluorescence spectroscopic studies of **T1** interactions with nucleic acids*

The detailed fluorescence properties of **T1** with various G-quadruplexes and other nucleic acids were explored via a fluorescence titration assay. As shown in Fig. 5A, **T1** alone in buffer displayed a weak fluorescence emission. With the gradual addition of G-quadruplex DNA Pu27, the emission peak at approximately 558 nm was significantly enhanced. Such resulting fluorescence was stable for at least 1 h (Fig. S3, Supplementary Data). The significant fluorescence was also observed when **T1** was treated with the G-quadruplexes, RET, bcl-2, c-kit2 and c-kit1, which have all been determined to form a parallel structure (Fig. 5B). In contrast, we observed a much weaker fluorescence enhancement for the antiparallel G-quadruplexes htg21 and TBA under our experimental conditions. Additionally, a negligible fluorescence was also observed when titrating **T1** with double-stranded DNA (ds26 and hairpin) and single-stranded DNA (mut-Pu27 and mut-htg21). This trend in fluorescence intensities was observed by the naked eye under UV light (Fig. S4, Supplementary Data).

To further ascertain the selective fluorescence response of **T1**, we employed a competition experiment, in which the ability of **T1** to retain an enhanced fluorescence intensity with the addition of G-quadruplex Pu27 was challenged by single-stranded or double-stranded DNA competitor. As shown in Fig. 6, when gradually adding the G-quadruplex Pu27 into the solution containing 5 μM **T1** and 25 μM single-stranded DNA mut-htg21, the enhanced fluorescence emissions were practically identical to those in the experiment without a competitor. Similar results could be found when using double-stranded DNA hairpin instead of single-stranded DNA. These results demonstrated the promising potential of **T1** to serve as a promising G-quadruplex fluorescent probe even in a competitive environment.

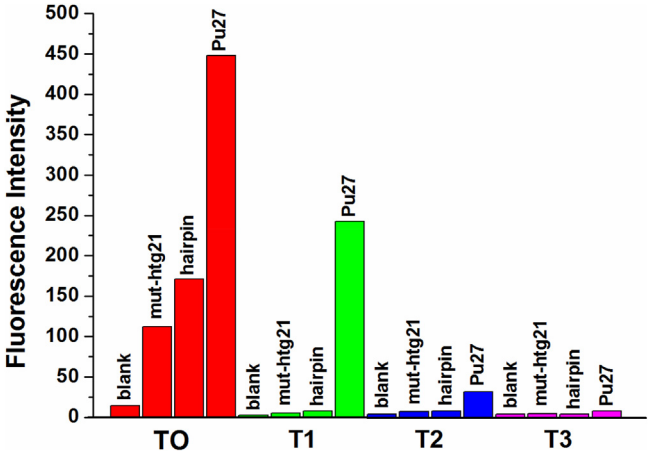

Fig. 4. Fluorescence responses of 0.5 μM of **TO** to 2 μM of different oligonucleotides ($\lambda_{ex}/\lambda_{em}$ = 485/530 nm) and 5 μM of **T1**, **T2**, and **T3** to 20 μM of different oligonucleotides ($\lambda_{ex}/\lambda_{em}$ = 480/558 nm) in 10 mM of Tris–HCl buffer and 100 mM of KCl at a pH of 7.2.

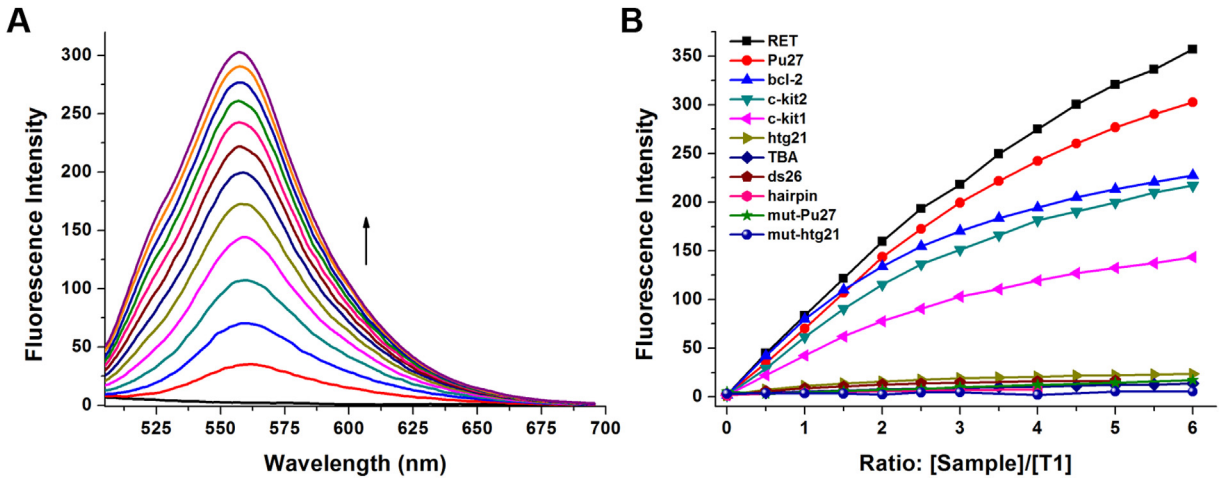

Fig. 5. (A) Fluorescence titration of 5 μM of **T1** with stepwise addition of the G-quadruplex-forming oligonucleotide (Pu27, arrows: 0–6 mol equiv.) in 10 mM of Tris–HCl buffer and 100 mM of KCl at a pH of 7.2. (B) The fluorescence intensity enhancement of 5 μM of **T1** at 558 nm against the ratio of [Sample]/[**T1**], λ_{ex} = 480 nm.

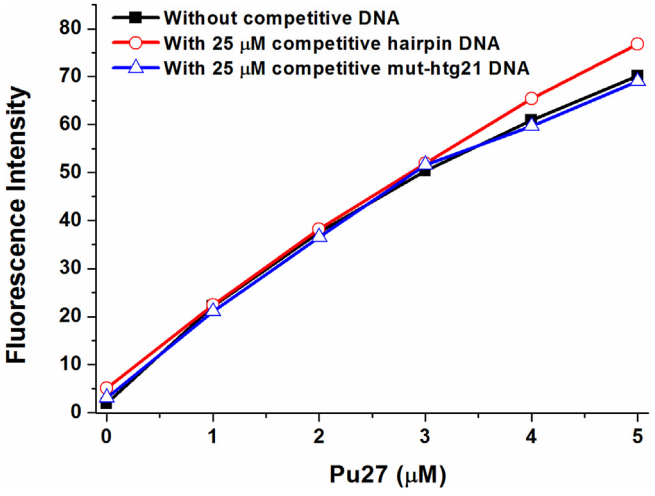

Fig. 6. Fluorescence titration of 5 μM **T1** with the stepwise addition of the G-quadruplex-forming oligonucleotide Pu27 without and with 25 μM double-stranded DNA hairpin or single-stranded DNA mut-htg21 in 10 mM of Tris–HCl buffer and 100 mM of KCl at a pH of 7.2.

Table 2
The fluorescence quantum yields of **TO** and **T1** with different nucleic acids.

Sample	Φ_F
$\mathbf{T1}_{Tris}$	0.001
$\mathbf{T1}_{RET}$	0.047
$\mathbf{T1}_{Pu27}$	0.046
$\mathbf{T1}_{bcl-2}$	0.036
$\mathbf{T1}_{c-kit2}$	0.020
$\mathbf{T1}_{c-kit1}$	0.032
$\mathbf{T1}_{htg21}$	0.004
$\mathbf{T1}_{TBA}$	0.002
$\mathbf{T1}_{ds26}$	0.002
$\mathbf{T1}_{hairpin}$	0.002
$\mathbf{T1}_{mut-Pu27}$	0.002
$\mathbf{T1}_{mut-htg21}$	0.001
$\mathbf{TO}_{Tris}$	0.004
$\mathbf{TO}_{Pu27}$	0.604
$\mathbf{TO}_{htg21}$	0.219
$\mathbf{TO}_{TBA}$	0.153
$\mathbf{TO}_{ds26}$	0.327
$\mathbf{TO}_{mut-Pu27}$	0.203
$\mathbf{TO}_{mut-htg21}$	0.197

The fluorescence quantum yield values of **T1** with different nucleic acids are summarized in Table 2. Notably, these values were consistent with the results for fluorescence titration, showing that the fluorescence emission enhancement was always more pronounced for the parallel G-quadruplex structures (RET, Pu27, bcl-2, c-kit2 and c-kit1). The quantum yield of **T1** for the G-quadruplex Pu27 was 0.046. This value was approximately 12 times higher than the value for the antiparallel G-quadruplex htg21, approximately 23 times higher than that of the antiparallel G-quadruplex TBA, approximately 23 times higher than that of the double-stranded ds26, and approximately 46 times higher than that of the single-stranded mut-htg21. In contrast, the quantum yields of **TO** for different nucleic acids were similar. The quantum yield of **TO** for the G-quadruplex Pu27 was 0.604, which was only approximately 2–4 times higher than the values for the antiparallel G-quadruplexes or double-stranded and single-stranded DNA. All of these results suggested that introduction of the hydrocarbon ring onto **TO** significantly improved its selectivity for G-quadruplexes, especially for the parallel structures. However, this modification reduced the quantum yield of **TO**.

In addition to the fluorescence quantum yield, we also investigated the detection limits of **T1** for different G-quadruplex. The LOD values were calculated on the basis of the equation $LOD = K \times S_b/m$ [40]. The K value is generally taken to be 3 according to the International Union of Pure and Applied Chemistry (IUPAC) recommendation. The S_b value represents the standard deviation for multiple measurements (n = 20) of blank solution. The m value is the slope of the calibration curve, which is derived from the linear range of the **T1** fluorescence titration curve with different nucleic acids and represents the sensitivity of this method (Fig. S5, Supplementary Data). The corresponding LOD values of **T1** for G-quadruplex Pu27, bcl-2, c-kit1, c-kit2 and RET were 15.2 nM, 16.7 nM, 31.8 nM, 21.8 nM and 16.0 nM, respectively.

3.5. PAGE studies

Encouraged by the significant and selective fluorescence enhancement of **T1** binding with G-quadruplex DNA, we were interested in the practical application of **T1** and then investigated its performance in staining G-quadruplex bands after gel electrophoresis. G-quadruplex DNA Pu27, double-stranded DNA hairpin and single-stranded DNA mut-htg21 were employed in the native

PAGE experiments. After electrophoresis, the polyacrylamide gel was immersed in 30 μmol/L **T1** staining solution for 20 min. As shown in Fig. 7, clear fluorescence band corresponding to G-quadruplex Pu27 was observed, and the bands of double-stranded DNA and single-stranded DNA were hardly detectable. Then, the PAGE experiment was repeated by using commercial GelRed stain as a benchmark. Compared with **T1**, GelRed was a stain for all types of nucleic acids. Collectively, these results demonstrated the feasibility of using **T1** as selective fluorescent stain for G-quadruplexes.

3.6. SPR studies

T1 exhibited a significantly improved selectivity for the G-quadruplexes compared with **TO**. Therefore, it is important to determine the mechanism of these interactions. Thus, we then investigated the **T1** interactions with the G-quadruplexes using surface plasmon resonance (SPR) assays because the selectivity of a compound for a G-quadruplex is closely related to the affinity. The alternative biotinylated G-quadruplexes, Pu27, htg21 and double-stranded dsDNA and single-stranded ssDNA, were employed. As shown in Table 3, the binding affinities for the G-quadruplexes occurred in the following order: **TO** > **T1** > **T2** > **T3**. These findings were in agreement with the fluorescence enhancement trend of **TO** and **TO**-derived compounds in the presence of the G-quadruplexes. However, **TO** exhibited a high affinity not only for the G-quadruplexes but also for double-stranded and single-stranded DNA. In contrast, the binding of **T1** towards double-stranded and single-stranded DNA was extremely weak. Thus, this discrepancy may explain why **T1** could be used in the selective detection of G-quadruplexes. Notably, **T1** showed selective fluorescence response for the G-quadruplex, Pu27, with a strong discrimination against htg21, but their binding affinities were similar. Furthermore, the binding affinities of **T1**, **T2** and **T3** for Pu27 were similar, but only **T1** exhibited a significant fluorescence enhancement upon binding. These results suggested that the selective fluorescence response of **T1** may arise not only from the binding selectivity but also from other factors.

3.7. Molecular modeling studies

It has been reported that the fluorescence enhancement of **TO** for nucleic acids may be caused by conformational changes in the excited state of **TO**, most likely by the rotation restriction around the methine-bridge that separates the benzothiazole and quinolinium rings upon binding. In this case, the chromophore of **TO** is nearly planar. This locked planar conformation is the key factor that is responsible for its significant fluorescence emission and further twisting about the methine bridge beyond an interplanar angle of 60° would lead to its dark state [2,41]. In a previous study, we also demonstrated that the introduction of a hydrocarbon ring affected the planar state of an unfused aromatic chromophore [42]. Thus, we predicted the possibility that the planarity of **TO**-derived compounds upon their binding to G-quadruplexes may also impact their fluorescence emissions. Therefore, modeling studies were performed to understand the planarity of these compounds, and **TO** was used as a reference.

The structures of **TO** and **TO**-derived compounds were first constructed and optimized with GAUSSIAN using the HF/6−31G* basis set. The planarity of these compounds could be defined by measuring the torsion angle between the benzothiazole and quinolinium rings. As shown in Table 4, the torsion angles of **TO**, **T1**, **T2** and **T3** were 16.2°, 45.6°, 51.9°, 62.4°, respectively, indicating that increasing the hydrocarbon ring size resulted in a significantly decreased planarity of their unfused aromatic core. These data could explain the results observed in the self-aggregation measurement and SPR assay because the non-planar conformations of **T1**, **T2** and **T3** may not allow the self-aggregation and intercalative binding in the duplex DNA to occur.

Next, molecular models of **TO** and **TO**-derived compounds with G-quadruplexes were generated by docking studies. The parallel

Table 3
Equilibrium dissociation constant (K_D) determined by the SPR assay.

	K_D (μM)			
	Pu27	htg21	dsDNA	ssDNA
TO	0.138	0.525	0.996	0.887
T1	2.35	2.00	–[a]	–[a]
T2	2.38	11.9	–[a]	–[a]
T3	3.45	19.2	–[a]	–[a]

[a] No significant binding was found for addition of up to 20 μM ligand.

Table 4
Torsion angles of **TO** and the **TO**-derived compounds in the absence and in the presence of the G-quadruplexes.

	Torsion angle (°)		
	Alone	With G-quadruplex Pu24I	With G-quadruplex htg21
TO	16.2	19.36	26.01
T1	45.6	49.07	61.57
T2	51.9	58.04	79.94
T3	62.4	61.45	69.77

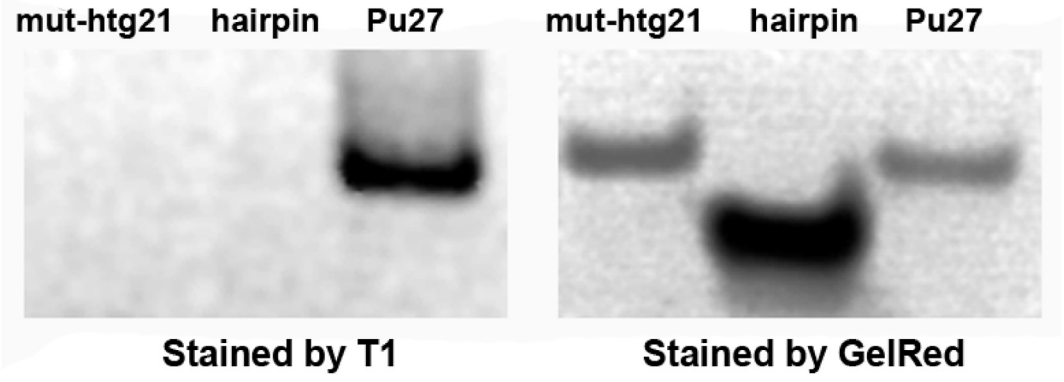

Fig. 7. Staining of G-quadruplex DNA Pu27, double stranded DNA hairpin and single-stranded DNA mut-htg21 by **T1** (A) and GelRed (B).

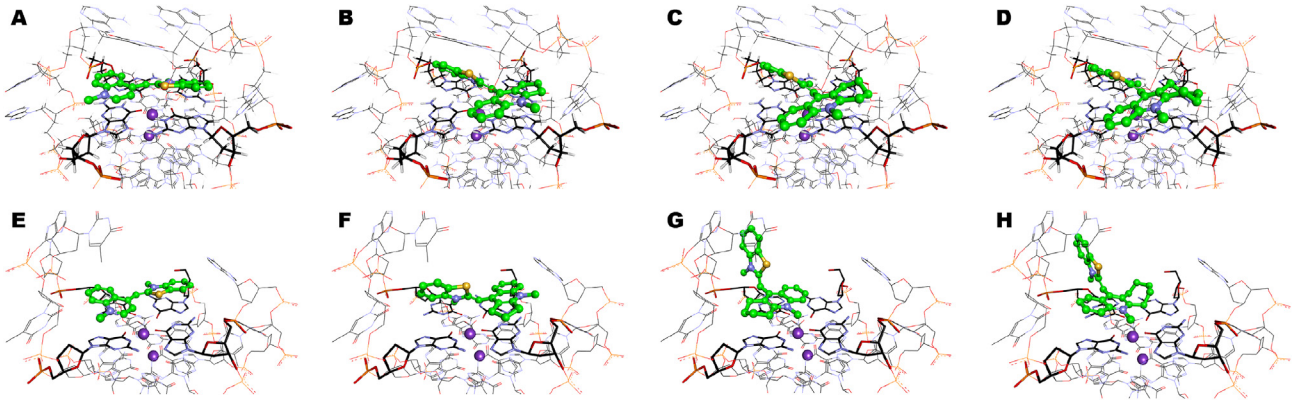

Fig. 8. Complex models of **TO** (A), **T1** (B), **T2** (C), **T3** (D) with Pu24I and complex models of **TO** (E), **T1** (F), **T2** (G), **T3** (H) with htg21.

Pu27-derived NMR G-quadruplex structure, Pu24I (PDB ID: 2A5R) [36], and an antiparallel NMR G-quadruplex structure for htg21 (PDB ID: 2MB3) were used as the templates [37]. As shown in Fig. 8, all of the compounds stacked on the G-quartet in a different manner. Considering their torsion angles in the presence of the G-quadruplexes (Table 4), **TO** was locked in an almost planar conformation, but the **TO**-derived compounds remained non-planar. Among the **TO**-derived compounds, the torsion angle of **T1** in the presence of the G-quadruplex, Pu24I, was much smaller than in the presence of the G-quadruplex, htg21. Moreover, the torsion angle was also much smaller than those of **T2** and **T3** in the presence of the G-quadruplex, Pu24I. Notably, these findings were in agreement with the trends observed in the fluorescence studies. Because the binding affinities of **T1**, **T2** and **T3** for Pu27 and **T1** for htg21 were similar, the discrepancy of their planarity might be the key factor responsible for the different fluorescence response upon binding to the G-quadruplexes.

4. Conclusions

The development of highly sensitive fluorescent probes to detect G-quadruplexes is of profound importance for a wide range of investigations. Although **TO** is non-selective for double-stranded and G-quadruplex nucleic acids, it may offer an attractive template for the design of selective G-quadruplex probes. Herein, we designed and synthesized a series of new **TO**-derived compounds by introducing a hydrocarbon ring. Among these compounds, **T1**, which includes a five-member ring compared with **TO**, was chosen as the most promising candidate due to its highly selective fluorescence response to G-quadruplexes. This simple structural modification to **TO** significantly improved its selectivity. Further study of the mechanism revealed that introduction of the hydrocarbon ring to **TO** significantly decreased the planarity of the unfused aromatic chromophore. Such non-planar conformations of **T1** may not allow the intercalative binding to duplex DNA. Notably, **T1** displayed considerable selectivity for parallel G-quadruplex structures with discrimination against some antiparallel G-quadruplexes. Moreover, we found that the quantum yields of **T1** were lower than those of **TO**. A discrepancy in the planarity upon its binding to different G-quadruplexes may also play an important role. In summary, we have successfully demonstrated that a simple structural modification to **TO** improves the selective detection performance of G-quadruplexes. The results will hopefully assist the search for a new generation of selective probes for G-quadruplexes. Further investigations on improving the sensitivity of **T1** for G-quadruplexes are now underway.

Acknowledgment

This work was financially supported by the National Natural Science Foundation of China (Nos. 81330077 and 21272291) and the Fundamental Research Funds for the Central Universities (Grants 14ykpy09 to J.-H. Tan).

Appendix A. Supplementary data

Supplementary data related to this article can be found at http://dx.doi.org/10.1016/j.dyepig.2015.11.010.

References

[1] Rye HS, Yue S, Wemmer DE, Quesada MA, Haugland RP, Mathies RA, et al. Stable fluorescent complexes of double-stranded DNA with bis-intercalating asymmetric cyanine dyes: properties and applications. Nucleic Acids Res 1992;20:2803–12.
[2] Nygren J, Svanvik N, Kubista M. The interactions between the fluorescent dye thiazole orange and DNA. Biopolymers 1998;46:39–51.
[3] Lee LG, Chen CH, Chiu LA. Thiazole orange: a new dye for reticulocyte analysis. Cytometry 1986;7:508–17.
[4] Rye HS, Quesada MA, Peck K, Mathies RA, Glazer AN. High-sensitivity two-color detection of double-stranded DNA with a confocal fluorescence gel scanner using ethidium homodimer and thiazole orange. Nucleic Acids Res 1991;19:327–33.
[5] Zhu H, Clark SM, Benson SC, Rye HS, Glazer AN, Mathies RA. High-sensitivity capillary electrophoresis of double-stranded DNA fragments using monomeric and dimeric fluorescent intercalating dyes. Anal Chem 1994;66:1941–8.
[6] Hoevelmann F, Gaspar I, Ephrussi A, Seitz O. Brightness enhanced DNA FIT-probes for wash-free RNA imaging in tissue. J Am Chem Soc 2013;135:19025–32.
[7] Monchaud D, Allain C, Teulade-Fichou M-P. Development of a fluorescent intercalator displacement assay (G4-FID) for establishing quadruplex-DNA affinity and selectivity of putative ligands. Bioorg Med Chem Lett 2006;16:4842–5.
[8] Monchaud D, Allain C, Teulade-Fichou MP. Thiazole orange: a useful probe for fluorescence sensing of G-quadruplex-ligand interactions. Nucleosides Nucleotides Nucleic Acids 2007;26:1585–8.
[9] Burge S, Parkinson GN, Hazel P, Todd AK, Neidle S, Quadruplex DNA. sequence, topology and structure. Nucleic Acids Res 2006;34:5402–15.
[10] Bochman ML, Paeschke K, Zakian VA. DNA secondary structures: stability and function of G-quadruplex structures. Nat Rev Genet 2012;13:770–80.
[11] Karsisiotis AI, Hessari NMa, Novellino E, Spada GP, Randazzo A, Webba da Silva M. Topological characterization of nucleic acid G-quadruplexes by UV absorption and circular dichroism. Angew Chem Int Ed 2011;50:10645–8.
[12] Davis JT. G-quartets 40 years later: from 5′-GMP to molecular biology and supramolecular chemistry. Angew Chem Int Ed 2004;43:668–98.
[13] Balasubramanian S, Hurley LH, Neidle S. Targeting G-quadruplexes in gene promoters: a novel anticancer strategy? Nat Rev Drug Discov 2011;10:261–75.
[14] Xiong Y-X, Huang Z-S, Tan J-H. Targeting G-quadruplex nucleic acids with heterocyclic alkaloids and their derivatives. Eur J Med Chem 2015;97:538–51.
[15] Ma D-L, Chan DS-H, Yang H, He H-Z, Leung C-H. Luminescent G-quadruplex probes. Curr Pharm Des 2012;18:2058–75.
[16] Vummidi BR, Alzeer J, Luedtke NW. Fluorescent probes for G-quadruplex structures. ChemBioChem 2013;14:540–58.

[17] Largy E, Granzhan A, Hamon F, Verga D, Teulade-Fichou M-P. Visualizing the quadruplex: from fluorescent ligands to light-up probes. Top Curr Chem 2013;330:111–78.
[18] Chan DS-H, Yang H, Kwan MH-T, Cheng Z, Lee P, Bai L-P, et al. Structure-based optimization of FDA-approved drug methylene blue as a c-myc G-quadruplex DNA stabilizer. Biochimie 2011;93:1055–64.
[19] He H-Z, Leung K-H, Wang W, Chan DS-H, Leung C-H, Ma D-L. Label-free luminescence switch-on detection of T4 polynucleotide kinase activity using a G-quadruplex-selective probe. Chem Commun 2014;50:5313–5.
[20] Laguerre A, Stefan L, Larrouy M, Genest D, Novotna J, Pirrotta M, et al. A twice-as-smart synthetic G-quartet: PyroTASQ is both a smart quadruplex ligand and a smart fluorescent probe. J Am Chem Soc 2014;136:12406–14.
[21] Lu L, Shiu-Hin Chan D, Kwong DWJ, He H-Z, Leung C-H, Ma D-L. Detection of nicking endonuclease activity using a G-quadruplex-selective luminescent switch-on probe. Chem Sci 2014;5:4561–8.
[22] Zhang L, Er JC, Ghosh KK, Chung WJ, Yoo J, Xu W, et al. Discovery of a structural-element specific G-quadruplex "light-up" probe. Sci Rep 2014;4:3776.
[23] Bhasikuttan AC, Mohanty J. Targeting G-quadruplex structures with extrinsic fluorogenic dyes: promising fluorescence sensors. Chem Commun 2015;51:7581–97.
[24] Doria F, Oppi A, Manoli F, Botti S, Kandoth N, Grande V, et al. A naphthalene diimide dyad for fluorescence switch-on detection of G-quadruplexes. Chem Commun 2015;51:9105–8.
[25] Laguerre A, Hukezalie K, Winckler P, Katranji F, Chanteloup G, Pirrotta M, et al. Visualization of RNA-quadruplexes in live cells. J Am Chem Soc 2015;137:8521–5.
[26] Gabelica V, Maeda R, Fujimoto T, Yaku H, Murashima T, Sugimoto N, et al. Multiple and cooperative binding of fluorescence light-up probe thioflavin T with human telomere DNA G-quadruplex. Biochemistry 2013;52:5620–8.
[27] Mohanty J, Barooah N, Dhamodharan V, Harikrishna S, Pradeepkumar PI, Bhasikuttan AC. Thioflavin T as an efficient inducer and selective fluorescent sensor for the human telomeric G-quadruplex DNA. J Am Chem Soc 2013;135:367–76.
[28] Renaud de la Faverie A, Guedin A, Bedrat A, Yatsunyk LA, Mergny J-L. Thioflavin T as a fluorescence light-up probe for G4 formation. Nucleic Acids Res 2014;42:e65.
[29] Yang P, De Cian A, Teulade-Fichou M-P, Mergny J-L, Monchaud D. Engineering bisquinolinium/thiazole orange conjugates for fluorescent sensing of G-quadruplex DNA. Angew Chem Int Ed 2009;48:2188–91.
[30] Lu Y-J, Yan S-C, Chan F-Y, Zou L, Chung W-H, Wong W-L, et al. Benzothiazole-substituted benzofuroquinolinium dye: a selective switch-on fluorescent probe for G-quadruplex. Chem Commun 2011;47:4971–3.
[31] Yan J-W, Ye W-J, Chen S-B, Wu W-B, Hou J-Q, Ou T-M, et al. Development of a universal colorimetric indicator for G-quadruplex structures by the fusion of thiazole orange and isaindigotone skeleton. Anal Chem 2012;84:6288–92.
[32] Tan J-H, Ou T-M, Hou J-Q, Lu Y-J, Huang S-L, Luo H-B, et al. Isaindigotone derivatives: a new class of highly selective ligands for telomeric G-quadruplex DNA. J Med Chem 2009;52:2825–35.
[33] Hou J-Q, Chen S-B, Tan J-H, Ou T-M, Luo H-B, Li D, et al. New insights into the structures of ligand-quadruplex complexes from molecular dynamics simulations. J Phys Chem B 2010;114:15301–10.
[34] Yan J-W, Chen S-B, Liu H-Y, Ye W-J, Ou T-M, Tan J-H, et al. Development of a new colorimetric and red-emitting fluorescent dual probe for G-quadruplex nucleic acids. Chem Commun 2014;50:6927–30.
[35] Klochko OP, Fedyunyayeva IA, Khabuseva SU, Semenova OM, Terpetschnig EA, Patsenker LD. Benzodipyrrolenine-based biscyanine dyes: synthesis, molecular structure and spectroscopic characterization. Dyes Pigments 2010;85:7–15.
[36] Phan AT, Kuryavyi V, Gaw HY, Patel DJ. Small-molecule interaction with a five-guanine-tract G-quadruplex structure from the human MYC promoter. Nat Chem Biol 2005;1:167–73.
[37] Chung WJ, Heddi B, Tera M, Iida K, Nagasawa K, Phan AT. Solution structure of an intramolecular $(3 + 1)$ human telomeric G-quadruplex bound to a telomestatin derivative. J Am Chem Soc 2013;135:13495–501.
[38] Lau V, Heyne B. Calix[4]arene sulfonate as a template for forming fluorescent thiazole orange H-aggregates. Chem Commun 2010;46:3595–7.
[39] Dutta Choudhury S, Bhasikuttan AC, Pal H, Mohanty J. Surfactant-induced aggregation patterns of thiazole orange: a photophysical study. Langmuir 2011;27:12312–21.
[40] Hu M-H, Chen S-B, Guo R-J, Ou T-M, Huang Z-S, Tan J-H. Development of a highly sensitive fluorescent light-up probe for G-quadruplexes. Analyst 2015;140:4616–25.
[41] Silva GL, Ediz V, Yaron D, Armitage BA. Experimental and computational investigation of unsymmetrical cyanine dyes: understanding torsionally responsive fluorogenic dyes. J Am Chem Soc 2007;129:5710–8.
[42] Hou J-Q, Tan J-H, Wang X-X, Chen S-B, Huang S-Y, Yan J-W, et al. Impact of planarity of unfused aromatic molecules on G-quadruplex binding: learning from isaindigotone derivatives. Org Biomol Chem 2011;9:6422–36.